Resource

Structure

Manipulation of Subunit Stoichiometry in Heteromeric Membrane Proteins

Graphical Abstract

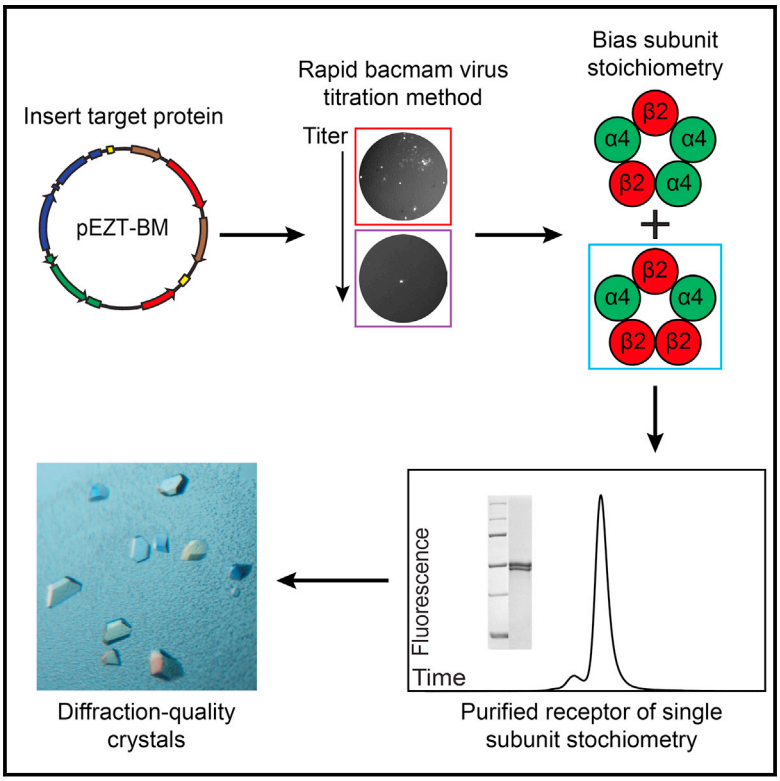

Highlights

- Streamlined bacmam virus titration method
- Fluorescent protein fusion approach for estimation of subunit ratio in a heteromer
- Expression and crystallization of a defined nicotinic receptor stoichiometry

Authors

Claudio L. Morales-Perez, Colleen M. Noviello, Ryan E. Hibbs

Correspondence

ryan.hibbs@utsouthwestern.edu

In Brief

Morales-Perez et al. developed a pair of methods to efficiently express defined stoichiometries of heteromeric membrane proteins. Application of this approach to a nicotinic acetylcholine receptor that can assemble in multiple functional ratios of subunits has yielded diffraction-quality crystals of the receptor.

Morales-Perez et al., 2016, Structure *24*, 797–805
May 3, 2016 ©2016 Elsevier Ltd All rights reserved
http://dx.doi.org/10.1016/j.str.2016.03.004

Structure
Resource

Manipulation of Subunit Stoichiometry in Heteromeric Membrane Proteins

Claudio L. Morales-Perez,[1] Colleen M. Noviello,[1] and Ryan E. Hibbs[1,*]
[1]Departments of Neuroscience and Biophysics, University of Texas Southwestern Medical Center, Dallas, TX 75390, USA
*Correspondence: ryan.hibbs@utsouthwestern.edu
http://dx.doi.org/10.1016/j.str.2016.03.004

SUMMARY

The ability of oligomeric membrane proteins to assemble in different functional ratios of subunits is a common feature across many systems. Recombinant expression of hetero-oligomeric proteins with defined stoichiometries facilitates detailed structural and functional analyses, but remains a major challenge. Here we present two methods for overcoming this challenge: one for rapid virus titration and another for stoichiometry determination. When these methods are coupled, they allow for efficient dissection of the heteromer stoichiometry problem and optimization of homogeneous protein expression. We demonstrate the utility of the methods in a system that to date has proved resistant to atomic-scale structural study, the nicotinic acetylcholine receptor. Leveraging these two methods, we have successfully expressed, purified, and grown diffraction-quality crystals of this challenging target.

INTRODUCTION

Most trimeric, tetrameric, pentameric, and hexameric families of human membrane proteins are populated by heteromeric members (Changeux and Edelstein, 2005; Yang et al., 2012; Durisic et al., 2012; Barrera et al., 2005; Miles et al., 2013; Sigel and Steinmann, 2012; Saul et al., 2013; Bartoi et al., 2014; Meltzer et al., 2007; Traynelis et al., 2010; Cooper and Jan, 2003, Robbins, 2001; Craven and Zagotta, 2006; Saez et al., 2003). Heteromeric channel assemblies have, with very few exceptions, resisted atomic-scale structural analysis (Karakas and Furukawa, 2014; Lee et al., 2014). Within a protein family the different heteromeric assemblies exhibit finely tuned functional properties and often play distinct and important physiological roles. The prototypical cell surface receptor is the nicotinic acetylcholine (ACh) receptor, which is a ligand-gated ion channel important in fast chemical neurotransmission (Changeux and Edelstein, 2005). Defects in nicotinic receptor function are linked to neuromuscular disorders, mental illness, neurodegenerative disease, and addiction (Engel et al., 2015; Dineley et al., 2015). Human nicotinic receptors are pentameric and assemble in a large but restricted number of combinations from a panel of 16 homologous subunits. The vast majority of the subunits must assemble with other subunits as obligate heteromeric complexes. This feature presents an additional level of complexity when approaching structural and functional studies of the nicotinic receptor family. The most abundant nicotinic receptor in the brain is the $\alpha4\beta2$ subtype, which is the target of this case study.

The $\alpha4\beta2$ receptor is a particularly daunting molecule for structural analysis, as it is known to assemble into pentamers with variable ratios of the $\alpha4$ and $\beta2$ subunits (Anand et al., 1991; Cooper et al., 1991; Zwart and Vijverberg, 1998). Elegant studies using metabolic labeling (Nelson et al., 2003) and expression of concatameric receptors (Carbone et al., 2009; Zhou et al., 2003) provided convincing evidence that only two stoichiometries successfully assemble, $(\alpha4)_2(\beta2)_3$ and $(\alpha4)_3(\beta2)_2$, each with a single ordering of subunits around the pentameric ring. These two stoichiometries exhibit different sensitivities to ACh and nicotine and have distinct ion selectivities and single-channel conductances (Nelson et al., 2003; Moroni et al., 2006). There is good evidence that both stoichiometries are expressed in the brain (Marks et al., 1999, 2007, 2010) and that overall levels of the receptor protein are dramatically increased in smokers' brains (Perry et al., 1999). The "high-affinity" stoichiometry with three copies of the β subunit is selectively upregulated by nicotine in a range of systems (Moroni et al., 2006; Lester et al., 2009; Buisson and Bertrand, 2001; Kuryatov et al., 2005; Nelson et al., 2003; Srinivasan et al., 2012). Thus, the $\alpha4\beta2$ receptor assembles into limited pentameric stoichiometries, with distinct functional properties of physiological relevance.

An important goal is to obtain atomic-resolution structures of the different stoichiometries of this receptor to provide a framework for understanding mechanisms of heteromer assembly, ligand recognition, and ion permeation. Whether by single-particle cryoelectron microscopy or crystallographic methods, achieving this goal requires the ability to isolate a pure or nearly pure stoichiometric population. Obtaining a pure population requires first the ability to measure stoichiometry in a population, and second the ability to express or purify only one receptor stoichiometry. Here, we describe a new rapid viral titration system and fluorescence-based assay for stoichiometry that have allowed us to obtain to our estimate a pure stoichiometric population of the $\alpha4\beta2$ receptor. Utilizing these new techniques, we have been able to produce diffraction-quality crystals of this protein. The assays and approach are in principle generalizable to many systems, including protein complexes and situations whereby subunit stoichiometry is unknown. The titration assay is useful for any group working with bacmam virus but could easily be adapted for other virus types. The fluorescence-based assay for stoichiometry is adaptable across both prokaryotic and other eukaryotic expression systems.

 ©2016 Elsevier Ltd All rights reserved

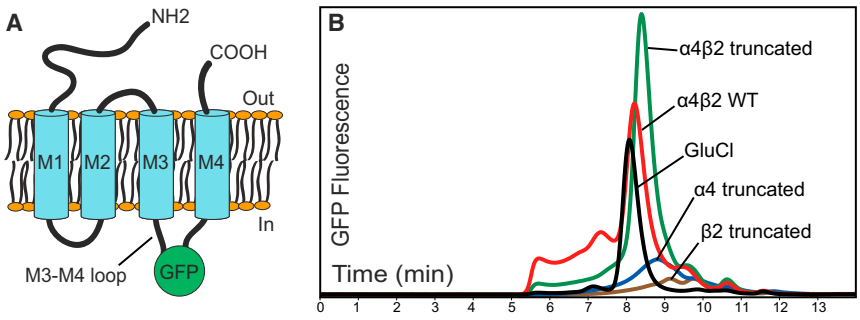

Figure 1. Expression of Receptor Constructs by Transient Transfection

(A) Schematic of the topology of nicotinic receptors. All receptor constructs were subcloned into the pEZT-BM vector and contain GFP spliced into the M3-M4 intracellular loop.

(B) GnTI$^-$ HEK cells in a 12-well dish were transfected; 3 days after transfection the cells were harvested and solubilized in a detergent solution (see Experimental Procedures). The crude extract was analyzed by FSEC, monitoring GFP fluorescence (λ_{exc}, 483 nm; λ_{em}, 510 nm). FSEC separations were performed using an SRT SEC-500 column (Sepax Technologies) with a flow rate of 0.35 ml/min. Comparison of $\alpha4\beta2$ with our reference for a crystallizable pentameric receptor, the homomeric *Caenorhabditis elegans* glutamate-gated chloride channel α (GluCl) (Hibbs and Gouaux, 2011), indicates that the major species of the $\alpha4\beta2$ receptor elutes at a volume consistent with pentameric assembly. We observed improved expression and monodispersity with the constructs containing M3-M4 loop truncations compared with the full-length, wild-type (WT) constructs. Results from transfection of $\alpha4$ or $\beta2$ alone suggest that the individual subunits do not readily assemble as homopentamers. Observation of epifluorescence from the single-subunit transfections revealed intensely fluorescent intracellular punctae and dramatically reduced plasma membrane fluorescence compared with co-transfections of both subunits. Based on FSEC results, these intracellular punctae likely represent aggregated and insoluble receptor subunits.

RESULTS

Expression Systems

Before tackling the stoichiometry problem, we first needed to identify an appropriate expression system for the $\alpha4\beta2$ receptor. For the purposes of small-scale screening, we inserted the enhanced GFP into the large cytoplasmic M3-M4 loop of the $\alpha4$ and $\beta2$ subunits (Figure 1A). Insertion of fluorescent proteins into this location has been shown to not affect receptor trafficking or function (Nashmi et al., 2003). This GFP fusion approach allowed us to assess expression level and receptor monodispersity in crude cell extracts by fluorescence-detection size-exclusion chromatography (FSEC) (Kawate and Gouaux, 2006). In initial expression trials, we found that the human $\alpha4\beta2$ receptor was robustly expressed by transient transfection of HEK293 cells (Figure 1B). In these transient transfections we used a 1:1 ratio of DNA for each subunit. Among HEK cell lines we chose the GnTI$^-$ derivative because it produces proteins with homogeneous, high-mannose N-glycans (Reeves et al., 2002). Thus, the use of this cell line allows for production of more homogeneous glycoproteins and carbohydrates that can be cleaved more efficiently, both of which are desirable for crystallization. As a long-term goal of ours is structural characterization of the receptor, we explored truncations of the M3-M4 loop to remove regions predicted to be disordered. Figure 1B shows improved expression and monodispersity in a promising truncation construct.

Several viable options exist for large-scale expression in GnTI$^-$ cells that have already shown promise for mammalian ligand-gated ion channels. These include transient transfection (Aricescu et al., 2006; Seiradake et al., 2015; Hacker et al., 2013), generation of inducible stable cell lines (Seiradake et al., 2015; Chaudhary et al., 2012), and transduction with "bacmam" baculovirus (Dukkipati et al., 2008; Goehring et al., 2014). We targeted the bacmam system because of its increased efficiency compared with generating stable cell lines and increased yield, in our hands, compared with transient transfections. The ability of baculovirus to infect a variety of mammalian cell types including HEK cells was discovered ~20 years ago (Boyce and Bucher, 1996; Hofmann et al., 1995). Shortly thereafter it was demonstrated that protein transduction in mammalian cells by baculovirus could be accomplished by replacing the traditional insect cell promoter in the baculovirus transfer plasmid with a mammalian promoter (Condreay et al., 1999). Furthermore, concentration of baculovirus or bacmam virus allows for very high MOI (Philipps et al., 2005), a tool for boosting protein expression with limited toxicity. The bacmam method and detailed protocols have recently been described in detail (Goehring et al., 2014). Here we focus on exploiting the bacmam system for expression of heteromeric membrane proteins with variable stoichiometries for structural studies.

Rapid Bacmam Titration System

We were initially motivated to develop an improved viral titration assay due to large variabilities in protein expression using different batches of virus. The desire to manipulate receptor stoichiometry provided further motivation to find an efficient way to determine viral potency. Existing baculovirus titration methods have significant drawbacks. Traditional plaque and endpoint dilution assays require 5–10 days for results, and alternatives that are faster count both infectious and non-infectious particles (Shen et al., 2002), or require maintenance of an additional cell line (Hopkins and Esposito, 2009), specialized equipment (Qi et al., 2015), or relatively expensive antibody-based reagents (Wang et al., 2013). In any major structural biology undertaking, many expression conditions and constructs need to be assayed; thus, any way to increase efficiency can dramatically increase the likelihood of success. Furthermore, we have discovered large variability in baculovirus titers. With an insect cell expression system this variable titer is less of a concern, because the baculovirus can replicate within the insect cells at the same time as producing protein. However, in the bacmam system the virus is replication incompetent in the expression host. Thus, a virus of known titer is required for consistent MOI to express protein.

We assembled a new bacmam expression vector to streamline the viral titration step and optimize viral production. The new vector is based on the backbone of the commercially available pFastBacDual vector (Figure 2A). In this vector we replaced the insect polyhedrin promoter with a cassette containing a cytomegalovirus (CMV) promoter, multiple-cloning site, and transcript-stabilizing elements. We placed a codon-optimized GFP gene following the insect p10 promoter in the reverse orientation

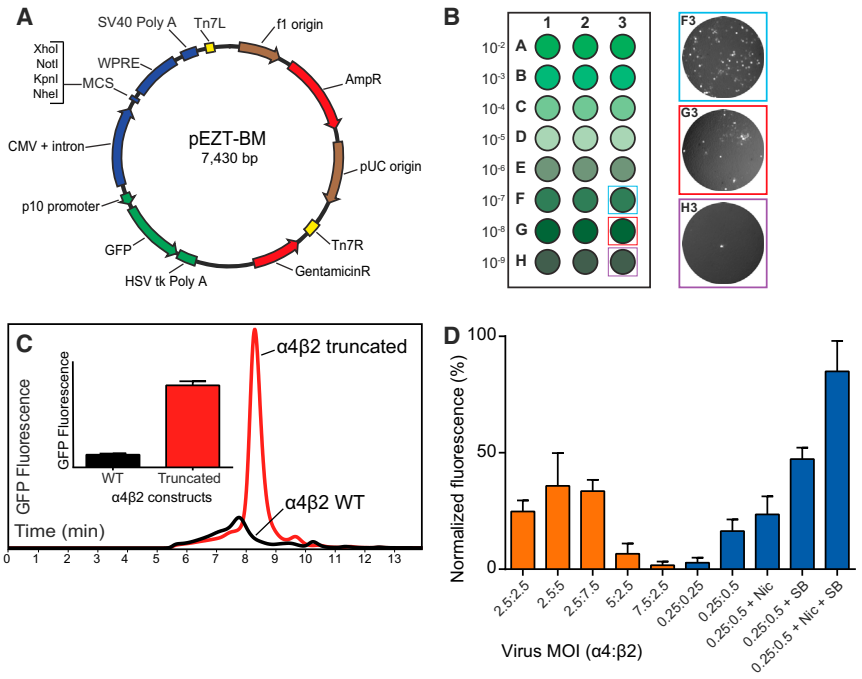

Figure 2. pEZT-BM Vector and Its Use in Transduction

(A) Map of the vector. The CMV promoter drives expression in mammalian cells of genes of interest cloned into the multiple-cloning site (MCS). The p10 promoter drives expression of GFP in Sf9 insect cells, which allows for monitoring of virus production and quantification of viral titer.

(B) Schematic and representative images from a serial titration.

(C) FSEC analysis of WT and truncation constructs of the α4β2 receptor after viral transduction of 1 ml cultures of GnTI$^-$ HEK cells; all constructs contain the intracellular GFP fusion. FSEC separations were performed as in Figure 1. The inset bar graph summarizes the results from three transductions.

(D) Comparison of expression levels after transduction of GFP fusions of truncated α4-GFP and β2-GFP constructs. Optimization of the viral ratio identified best expression from an MOI ratio of 1(α4):2(β2) (orange bars). Thereafter, different absolute MOIs ± 0.1 μM nicotine (Nic) and 3 mM sodium butyrate (SB) were explored to identify optimal expression conditions (blue bars).

Bar graphs in (C) and (D) present the mean values from three independent experiments; error bars denote SEM.

from the CMV promoter. This vector, which we call pEZT-BM (for easy-titer bacmam plasmid), can be used for several purposes. With genes inserted into the multi-cloning site, the plasmid can be used for traditional transient transfections in mammalian cells. The plasmid can also be used for the bac-to-bac method of making baculovirus (bacmam virus in this case) with no modifications from the commercial protocol. Finally, the titer of the virus can be monitored by fluorescence of infected Sf9 cells (Figure 2B) (Philipps et al., 2005). This last feature allows for monitoring of baculovirus production in real time under a fluorescence microscope and titration via a simple endpoint dilution assay. While many laboratories assume virus production peaks after 48 hr, we find variability in this assumed production time, and have been able to improve viral titers based on GFP fluorescence of virus-producing cells. Most importantly for the problem of stoichiometry, we are able to obtain reliable relative titers in 48 hr without the need for an additional cell line, plaque assay, or expensive commercial reagents. Indeed, our method is in essence a faster plaque assay, as we are measuring infectious units but using fluorescence as a readout instead of cell death. A fluorescent "plaque" can be seen in the upper right corner of well G3 in Figure 2B, with a bright central cell and fainter radial cells. A detailed titration protocol is described in Experimental Procedures.

Optimization of MOI for Expression

After obtaining the titer of pEZT-based bacmam viruses for α4-GFP and β2-GFP, we set out to identify optimal conditions for large-scale expression of the receptor. We first compared expression of the α4β2 wild-type (WT) and truncation constructs by transduction. This control experiment was done with the viruses in a 1:1 MOI ratio. These transduction results are shown in Figure 2C and demonstrate dramatically improved expression and monodispersity of the truncation construct compared with the WT construct. These relative improvements seen in the transduction experiment are even more impressive than those seen by transfection (Figure 1B). All further experiments to optimize expression were performed with the truncation construct.

We were next interested in determining the optimal MOI for each of the two subunits. We performed a series of small-scale transductions comparing different MOIs for each subunit along with the addition of chemical chaperones. The whole-cell extracts from these transductions were analyzed by FSEC at the appropriate wavelength for GFP. The relative peak heights of the pentamers are shown in Figure 2D. We consistently found that using more β than α virus resulted in higher overall pentamer expression level. We also found that we were able to minimize the consumption of virus by including nicotine, which is known to upregulate cell surface expression of the $(\alpha4)_2(\beta2)_3$ subtype of the receptor, and sodium butyrate, a histone deacetylase inhibitor that has been shown to boost recombinant expression of many proteins (Gorman et al., 1983). By systematically optimizing butyrate and nicotine concentrations with respect to viral MOI, we were able to decrease virus consumption 10-fold (Figure 2D, blue bars). It is important to note that these MOI values of <1 reflect MOI calculated from infection of Sf9 cells and thus serve only as a proxy for the MOI in GnTI$^-$ cells. Conditions around the "sweet spot" for expression are shown in Figure 2D. We also examined a broader range of butyrate concentrations and viral MOI and found that when using a relatively high MOI (>5), butyrate had a negative effect on expression level. Optimal transduction conditions for this protein include MOI values of 0.25 and 0.5 for the α4 and β2 subunit viruses, respectively, 0.1 mM nicotine and 3 mM sodium butyrate all added to the suspension culture at the time of transduction.

Stoichiometry Assay

We sought to develop a biochemical assay to measure the proportion of each subunit in our purified protein preparation. The

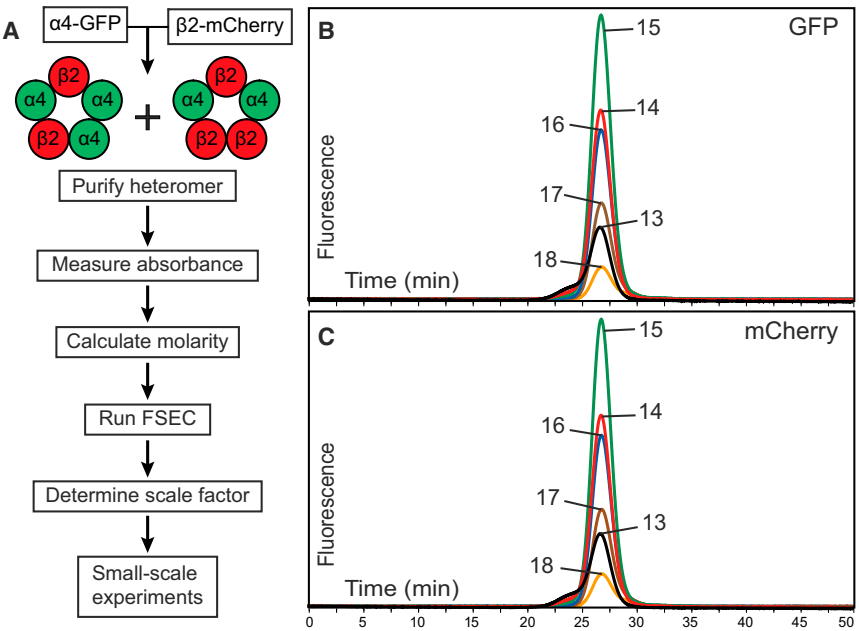

Figure 3. Stoichiometry Assay

(A) Flow chart outlining the assay as follows. (1) Titered virus for α4-GFP and β2-mCherry is used to transduce large-scale (1 l) expression of the receptor in suspension GnTI$^-$ HEK cells. (2) The receptor is purified from membranes via affinity chromatography and SEC. (3) The absorbance values of GFP (λ = 488 nm) and mCherry (λ = 587 nm) are measured for each pentameric SEC fraction (see Table S1). (4) The molarity of α4-GFP and β2-mCherry are calculated by dividing the absorbance values by their extinction coefficients. (5) A known amount of each SEC fraction is run in analytical FSEC, monitoring GFP and mCherry fluorescence (mCherry λ_{exc}, 587 nm; λ_{em}, 610 nm; for GFP as in Figure 1). (6) Scale factors are calculated by dividing the pentameric peak fluorescence amplitudes for GFP and mCherry in analytical FSEC by their respective molarities. These scale factors can then be used to back-calculate subunit molarities and thereby molar ratios in small-scale experiments analyzed simply by two-color FSEC.

(B and C) An example of the two-color FSEC for GFP and mCherry. FSEC separations were performed using a Superose 6 10/300 GL column (GE Healthcare) with a flow rate of 0.5 ml/min.

assay for stoichiometry needed to be efficient; ideally it would not require multiple purifications of the receptor so that many constructs and expression conditions could be examined in parallel on a small scale. To this end, we designed a two-color fluorescent protein fusion approach that required a single purification to standardize our fluorescence detectors, after which all experiments were performed in cell extracts from a 1 ml culture scale. A flow chart outlining the assay is shown in Figure 3A. To begin, we replaced the GFP in β2 with mCherry, selected because of good spectral separation from GFP (Shaner et al., 2005). We made bacmam virus for these two constructs, titered the viruses, and transduced GnTI$^-$ suspension cells with an MOI of 2.5 for each subunit (chronologically, this experiment was performed before we identified the improved expression conditions in Figure 2D). We purified the receptor using affinity chromatography against a C-terminal Strep-tag on the β2 subunit followed by size-exclusion chromatography (SEC). We next measured absorption of the GFP and mCherry chromophores for each pentameric SEC fraction. These values allowed us to estimate the molar concentration of each chromophore, and thereby each subunit, using the molar extinction coefficients of the chromophores. We then passed these SEC fractions over an analytical SEC column and monitored both GFP and mCherry fluorescence. From the peak fluorescence intensities at the pentamer elution volume, we calculated a scale factor to convert fluorescence values on our detectors to absolute molar concentrations. By dividing the molar concentrations of the two subunits, we determined the stoichiometric ratio of the two subunits. Example analytical two-color FSEC results are shown in Figures 3B and 3C. The estimated α/β subunit ratio in this purified preparation was 0.91 ± 0.03, which is consistent with a majority of the $(\alpha4)_2(\beta2)_3$ form but significant amounts of the $(\alpha4)_3(\beta2)_2$ form. Scale factor and stoichiometric determinations are shown in Table S1.

Expression of a Single α4β2 Receptor Subunit Stoichiometry

The results from our purification of the α4-GFP+β2-mCherry receptor indicated that we had isolated a population with mixed stoichiometries. Thus, we sought an approach to bias assembly of one pentameric stoichiometry over the other. A straightforward and generic approach for biasing assembly is to control the amount of DNA or virus used for each subunit to transiently express the protein. We screened a range of MOI ratios and nicotine concentrations on a 1 ml culture scale. After injecting detergent-solubilized cells over an analytical SEC column, we monitored GFP and mCherry fluorescence. We then calculated relative molarities of each subunit from the peak intensities at the pentamer elution volume using the scale factors determined above, and thereby determined the subunit ratio in the cell extracts (Figure 4 and Table S2). Because subunit ratio values are derived from the SEC peak amplitude of the pentameric species and not from a bulk solution in a cuvette, the effects of pentameric aggregates or breakdown products on the estimate of subunit stoichiometry are minimized. By varying the MOI ratio of the two pEZT viruses we were able to bias assembly toward the $(\alpha4)_2(\beta2)_3$ stoichiometry. We next took advantage of the property of nicotine to upregulate the $(\alpha4)_2(\beta2)_3$ stoichiometry. Using the best expression condition identified from Figure 2D and MOI ratios of 1:2 for α4/β2, we were able to obtain by our estimates a pure or nearly pure stoichiometry of two α4 subunits and three β2 subunits.

α4β2 Receptor Functional Validation, Purification, and Crystallization

We scaled up the expression conditions identified to maximize expression (Figure 2D) and stoichiometric homogeneity (Figure 4) to 1 l and purified protein via the same two-step procedure used for the GFP-mCherry fusion experiments (see Experimental

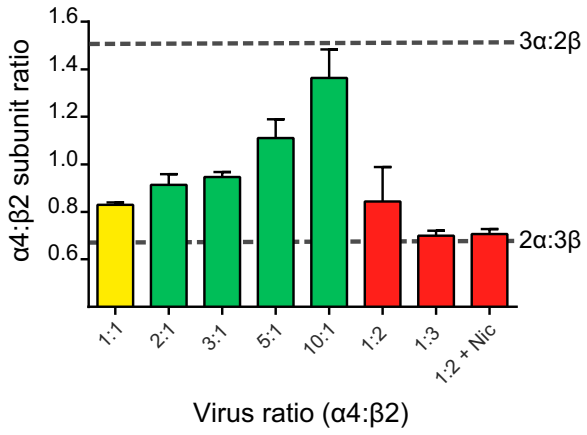

Figure 4. Small-Scale Experiments to Measure and Bias Stoichiometry

This bar graph presents calculated subunit molar ratios (y axis) based on the assay in Figure 3 versus different ratios of viral MOI in the presence of 3 mM sodium butyrate ± 0.1 μM nicotine. The transductions were performed on a 1 ml scale. A perfect 3α:2β stoichiometry would yield a ratio of 1.5 while the 2α:3β stoichiometry would yield a calculated ratio of 0.67. The results suggest that with equal amounts of virus for each subunit, the 2α:3β stoichiometry is predominantly expressed. The stoichiometry can be further biased toward the 2α:3β form by using more virus for the β subunit and including nicotine in culture. The results here are mean values ± SEM from three sets of transductions. Detailed results are shown in Table S2.

Procedures for details). For the purposes of crystallization we replaced the fluorescent proteins in both subunits with a thermostabilized protein, apocytochrome b(562)RIL ("bril"), which has been used to aid in crystallization of G-protein-coupled receptors (Chun et al., 2012). We validated the functionality of this truncated fusion protein by patch-clamp electrophysiology (Figure 5). In dose-response experiments in GnTI$^-$ cells transduced under the same conditions used to produce protein for crystallization, we observed a Hill coefficient of ~1.0, consistent with a homogeneous population of receptors. The previously published EC_{50} values for ACh at the WT receptor are ~4 μM and ~85 μM for the high-affinity and low-affinity stoichiometries, respectively (Carbone et al., 2009; Moroni et al., 2006; Nelson et al., 2003). Our measured EC_{50} value of ~30 μM is intermediate, which we ascribe to the significant construct modification used to promote crystallization. The results from a representative purification are shown in Figure 6A. Purified, concentrated protein was used to set up broad crystallization screens and conditions yielding crystals that were optimized by varying precipitant concentration. A promising crystal form is shown in Figure 6B, and representative diffraction with clearly visible reflections to 8 Å is shown in Figure 6C.

DISCUSSION

Utility of Titration Approach

We made several broadly useful findings in the course of optimizing expression of the α4β2 receptor using the bacmam system. The first relates to the importance of viral titration. Research groups working with baculovirus-mediated expression in insect cells can often maintain consistent, high-level protein expression without regularly determining viral titer. We found when implementing the bacmam system that expression levels were usually low and moreover were highly variable. Baculovirus replicates in Sf9 cells and thus the Sf9 cells will amplify the virus during protein expression. This spreading infection allows for a much lower MOI to be tolerated. Baculovirus (including bacmam virus) will not replicate in HEK cells, and thus the protein production depends much more directly on the amount of virus used to transduce expression. We regularly observe 10-fold and occasionally 100-fold variations in viral titer; without a titration assay, reliable expression of heteromeric assemblies in this system, in our hands, would not be feasible. Furthermore, by utilizing concentrated bacmam virus, proteins that were once thought impossible to express can be produced using higher MOIs. As measured on a separate target in the laboratory, we have seen expression increase with no detriment to the cells by using MOI as high as 25. When using high MOIs, however, virus consumption becomes a significant expense in terms of both media and time. We consistently find we are able to maintain high-level expression with dramatically lower MOIs simply by including histone deacetylase inhibitors such as sodium butyrate during transduction. We find that the optimal MOI and butyrate concentrations need to be identified empirically for each protein target; the assay presented here provides an efficient means for doing so.

Stoichiometry Assay

Functional, biochemical, and fluorescence-based approaches have been developed for counting subunits and measuring stoichiometry in living cells for numerous receptor families. We were interested, however, in an assay for purified protein, which would

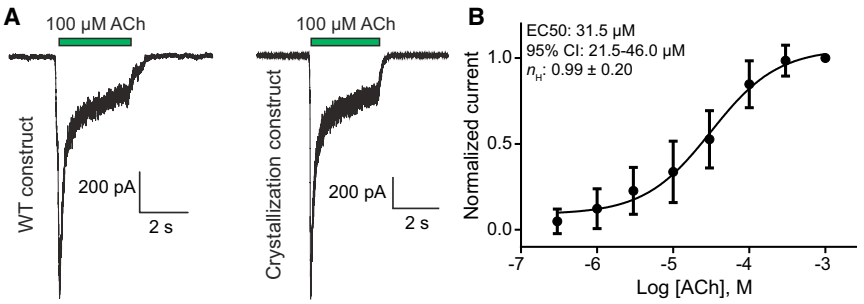

Figure 5. Functional Validation of the Crystallization Construct

(A) Whole-cell patch-clamp recordings obtained at −90 mV from adherent GnTI$^-$ cells transiently transfected with the WT and crystallization α4 and β2 constructs.

(B) Concentration-response relationship for ACh-induced activation of the crystallization constructs in virally transduced cells under the conditions used to produce protein for crystallization. The values shown are the normalized responses relative to that at 1 mM ACh. Error bars denote ±SEM from a minimum of two recordings from each of five cells. CI, confidence interval.

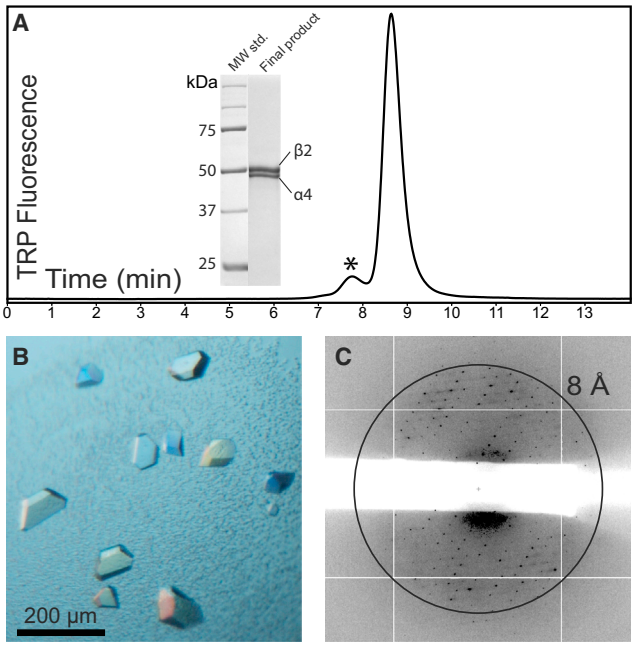

Figure 6. Purification and Crystallization

Optimal expression conditions identified in Figures 2D and 4 were scaled up with receptor lacking fluorescent protein fusions. In place of the fluorescent proteins, a crystallization chaperone, bril, was inserted in the same position. The same two-step purification strategy used in Figure 3 was applied to this modified receptor.

(A) The concentrated final product from purification, analyzed by Coomassie-stained SDS-PAGE and FSEC monitoring intrinsic tryptophan fluorescence (λ_{exc}, 280 nm; λ_{em}, 325 nm). FSEC was performed using an SRT SEC-500 column with a flow rate of 0.35 ml/min. The protein is pure; however, the sample is somewhat prone to concentration-dependent oligomerization or aggregation, indicated by the asterisk in the FSEC trace.

(B) An example of crystals of the receptor obtained from this purified protein preparation.

(C) Representative diffraction extending past 8 Å Bragg spacings. This crystal belongs to the *C*2 space group with unit cell dimensions of $a = 168$ Å, $b = 135$ Å, $c = 209$ Å, and $\beta = 113°$, which results in a solvent content of ~70% with one pentamer in the asymmetric unit.

give us information about the degree of homogeneity in a native preparation as close as reasonably achievable to the step of structural analysis. Moreover, we were interested in an assay that would inform conditions for large-scale expression but not require multiple purifications. We present a rapid, inexpensive assay that requires only one protein purification. When coupled with FSEC, many conditions can be tested in parallel to assess effects upon stoichiometry in a single experiment.

A potential source for error in our estimates of subunit concentrations in crude cell extracts relates to fluorescence resonance energy transfer (FRET) between the GFP and mCherry molecules. mCherry is a reasonably efficient FRET acceptor for GFP with a Förster radius of 52 Å (Akrap et al., 2010). We have not considered FRET in our calculations of scale factors used to convert fluorescence values to molar concentrations. If FRET is insignificant or is relatively constant between the two stoichiometries then our scale factors should not change, and there is no FRET-based error. However, a theoretical framework applied to single-molecule experiments suggests that FRET can vary significantly as the subunit stoichiometry varies (Srinivasan et al., 2012). To assess whether our small-scale experiments are accurately predictive of large-scale results, we performed a purification of α4-GFP+β2-mCherry using the same transduction conditions used for protein destined for crystallization, i.e., a condition we expected to give us an α/β molar ratio of 0.67, or 2α:3β. We measured absorbance of the two fluorescent protein chromophores to calculate the molar ratio in a manner that would not be affected by FRET. We obtained an α/β ratio of 0.67 ± 0.09, which suggests the small-scale experiments were successful in identifying conditions for purification-scale expression of a single stoichiometry, and that in this case, FRET variation was not affecting our estimate of stoichiometry for the 2α:3β stoichiometry. Importantly, for our purposes, an ability to track changes in apparent stoichiometry is sufficient. We are interested in homogeneity, and what we see is that as we vary the viral ratio, we can push the apparent stoichiometry to a certain point, but not past it. That point of "saturation" is in our case consistent with a homogeneous, single stoichiometry.

Conclusion

This combination of methods streamlines the bacmam system for recombinant expression of heteromeric proteins and protein complexes. The assays described here, however, are not limited to bacmam-mediated protein expression. For example, the parent vector we started with could easily be converted into a rapid-titer insect vector by placing GFP after the p10 promoter in the commercial starting vector and making no other modifications. The fluorescence-based assay for subunit stoichiometry could be used for protein produced in prokaryotic as well as other eukaryotic expression systems and could be expanded to more than two subunits by including additional fluorescent proteins as long as they maintain good spectral separation. Thus we are hopeful that the approach outlined here will be useful across a broad range of biological targets.

EXPERIMENTAL PROCEDURES

pEZT-BM Vector Design

The pFastBac Dual vector (Thermo Fisher Scientific) was used as a backbone for creation of the pEZT-BM vector. In the commercial vector we replaced the insect polyhedrin promoter with a cassette containing a CMV promoter, multiple-cloning site, and transcript-stabilizing elements. This cassette was derived from the pVLAD6 vector (Dukkipati et al., 2008) provided by Dr. Chris Garcia at Stanford University. The multiple-cloning sites were simplified to suit our purposes, as shown in Figure 2A. We placed a synthetic, codon-optimized enhanced GFP gene (Bio Basic) following the insect p10 promoter, which is in the reverse orientation from the CMV promoter. The p10 promoter drives the expression of GFP in insect cells, allowing real-time monitoring of baculovirus production and subsequent viral titration. The CMV promoter and downstream stabilizing elements drive expression of the recombinant protein in mammalian cells. The vector backbone contains the Tn7 transposition elements used for the bac-to-bac method of producing baculovirus. We use this vector for transient transfections of HEK cells and the bac-to-bac method to make bacmam virus following standard commercial protocols. The pEZT-BM vector is available from the Addgene plasmid repository (plasmid #74099).

Nicotinic Receptor Constructs and Small-Scale Screening

The human α4 and β2 subunit genes were provided by Dr. Jon Lindstrom at the University of Pennsylvania. Site-directed mutagenesis was used to make a silent single-nucleotide substitution in the α4 gene to remove an internal KpnI site. Next, PCR was used to add 5′ NotI and 3′ KpnI restriction sites

and a Kozak sequence; these sites were used for restriction digest and ligation-based subcloning into the pEZT-BM vector. Synthetic, codon-optimized GFP was inserted between the His551–Leu552 residues in the α4 mature sequence and His412–Met413 in the β2 subunit. In the truncated constructs, the residues Lys339–Pro536 are deleted in the α4 subunit and Cys331–Cys397 are deleted in the β2 subunit. The bril gene was obtained by synthesis, inserted into the same position as GFP in both α4 and β2, and an additional 19 residues surrounding bril were removed to promote crystallization (15 before and four after). The GluCl gene was provided by Henry Lester at Caltech via Addgene; in the construct we obtained, we replaced YFP with our synthetic GFP for the purposes of the transfection in Figure 1B. To purify the α4β2 receptor, we placed a Strep-tag (Maertens et al., 2015) at the C terminus of the β2 subunit. For stoichiometry analysis, the GFP copy in the truncated β2 construct was replaced with mCherry, which was provided by Dr. Roger Tsien at the University of California, San Diego. FSEC experiments were performed as follows. GnTI$^-$ HEK cells (ATCC; #CRL-3022) were added into 12-well tissue culture dishes and allowed to adhere for 24 hr, maintained at 37°C and 5% CO_2. The cells were transfected with 0.5 μg of each subunit using Lipofectamine 2000 (Thermo Fisher Scientific). After incubating for 72 hr at 30°C and 5% CO_2, the cells were harvested and solubilized with 20 mM Tris (pH 7.4), 150 mM NaCl, 1 mM PMSF (Sigma-Aldrich), and 40 mM dodecyl maltoside (DDM) detergent (Anatrace) for 40 min at 4°C. After centrifugation at 98,400 × *g* for 40 min at 4°C the supernatant was analyzed via SEC, detecting the GFP (λ_{exc}, 483 nm; λ_{em}, 510 nm) and mCherry (λ_{exc}, 587 nm; λ_{em}, 610 nm) fluorescence signals.

Virus Production and Titration

pEZT-BM constructs were transformed into DH10Bac cells (Thermo Fisher Scientific) to produce bacmid DNA as described in commercial protocols. For what we term "P1" virus production, a 35 mm well of Sf9 insect cells at a density of 1.0 × 10^6 cells/well was transfected with 5 μl (approximately 1 μg) of bacmid DNA using the commercial protocol for Cellfectin II (Thermo Fisher Scientific). The cells were incubated at 27°C until 90%–100% of the cells exhibited intense GFP fluorescence as monitored on a basic inverted fluorescence microscope. All culturing of Sf9 cells was performed in Sf-900 III SFM medium (Thermo Fisher Scientific). The virus-containing supernatant was collected, sterile filtered (0.22 μm), and added to Sf9 cells in suspension at a density of 1.0 × 10^6 cells/ml using a 1/500 volume of P1 virus. This secondary "P2" virus was produced at 27°C and 130 rpm until ~100% of the cells were fluorescent, typically 3–6 days later. The supernatant was collected, filtered, and concentrated (78,400 × *g* for 1 hr at 4°C, adapted from Philipps et al., 2005). The viral pellet was resuspended in 1/1,000 volume of Freestyle293 medium (Thermo Fisher Scientific) supplemented with 2% fetal bovine serum (Sigma-Aldrich). After resuspension, the secondary virus was sterile filtered (0.22 μm). We consistently find better than 99% recovery efficiency after virus concentration, based on comparing total infectious particle numbers before and after concentration. Viral titration was accomplished by an endpoint dilution assay (Flint, 2009). 100 μl per well of Sf9 cells was added into a black-walled 96-well culture plate (Corning #3603) at a density of 0.75 × 10^6 cells/well and allowed to adhere for 30 min at 27°C. A 10-fold dilution series (10^{-2} to 10^{-9}) was prepared using fresh tips for each dilution in triplicate with the filtered P2 virus stock (Figure 2B). After the incubation to allow cells to adhere, the medium in the 96-well culture plate was replaced with the dilution series. Cells were incubated for 48 hr at 27°C. Fluorescent cells were quantified and averaged across triplicate wells at the limiting dilution factor where fluorescent cells were still observed in order to calculate the concentration (titer) of infectious virus particles. The viral titer is calculated by dividing this average number of cells by their dilution factor and then multiplying by ten to account for viral particles per milliliter (as there is only 0.1 ml volume in the well). For example, if an average of 3.3 glowing cells is observed in row G of the tray, which is the 10^{-8} dilution row, then the titer would be 3 × 10^9 infectious units/ml. This value was then used as a proxy for determining the optimal infection conditions for HEK cells.

Protein Purification

One liter of GnTI$^-$ HEK cells was transduced with α4 and β2 pEZT-based bacmam viruses in the presence of 0.1 mM (−)-nicotine (Sigma-Aldrich) and 3 mM sodium butyrate (Sigma-Aldrich). After shaking for 72 hr at 30°C and 8% CO_2, the cells were harvested and lysed (Avestin EmulsiFlex-C5), followed by centrifugation at 9,800 × *g* for 15 min at 4°C. The supernatant was collected and centrifuged at 185,700 × *g* for 2 hr at 4°C to pellet the membranes. Membranes were homogenized, then solubilized with 20 mM Tris (pH 7.4), 150 mM NaCl, 40 mM DDM, 1 mM PMSF, 1 mM nicotine and 0.2 mM cholesteryl hemisuccinate (Anatrace) for 1 hr at 4°C. The solubilized protein was then purified by a Strep-Tactin (IBA) affinity column. Concentrated affinity fractions were incubated with endoglycosidase H overnight in a 1:8 w/w ratio of enzyme/receptor. Purification via preparative SEC followed on a Superose 10/300 GL column; fractions were pooled and concentrated to 1.6–1.9 mg/ml for direct use in crystallization. Identities of bands in SDS-PAGE (Figure 6A) were confirmed by tryptic digest and mass spectrometry.

Assay for Subunit Stoichiometry

The two-color FSEC approach utilizes the absorbance of the GFP and mCherry chromophores to calculate the molarity of the subunit that they are fused to. Thereafter, known molar quantities of the purified receptor are run in FSEC to determine a scale factor to correlate GFP and mCherry fluorescence values on a given instrument/detector with absolute molar concentration. These scale factors can then be used to convert fluorescence values from small-scale experiments with non-purified protein to calculate subunit concentrations and molar ratios.

We performed a purification of the α4-GFP+β2-mCherry receptor through the affinity and preparative SEC steps described in the previous section. For this purification we used a virus ratio of 1:1 for each subunit. The SEC fractions were analyzed via FSEC on a high-performance liquid chromatography system (Shimadzu) equipped with two fluorescence detectors in series. One detector was set to read GFP fluorescence and the other was set to detect mCherry fluorescence. The absorbance of each SEC fraction was measured at the maxima for the two fluorescent protein chromophores (GFP, 488 nm; mCherry, 587 nm). The absorbance of each fluorescent protein was divided by its respective extinction coefficient (GFP, 56,000 M^{-1} cm^{-1}; mCherry, 72,000 M^{-1} cm^{-1}) to calculate the molarity of each subunit (GFP for α4 and mCherry for β2). Then the fluorescence of the pentamer peak amplitude detected by FSEC (in μV) was divided by the molarity of each subunit to calculate the scale factor, in units of μV M^{-1}, for each fluorescent protein. Example calculations are shown in Table S1.

For small-scale experiments, 1 ml volumes of GnTI$^-$ HEK cells in suspension in 12-well dishes were transduced with different virus ratios of α4-GFP and β2-mCherry bacmam viruses, in the presence or absence of several additives. After shaking for 72 hr at 30°C and 8% CO_2, the cells were harvested and analyzed by FSEC, detecting the GFP and mCherry fluorescence signals. The molarity of each subunit was determined by dividing the peak fluorescence intensity for a given fluorophore by its scale factor; example calculations are shown in Table S2. This approach allowed for efficient estimation of the subunit molar ratio without the need to purify the protein for each expression condition.

Electrophysiology

To test the functionality of the crystallization construct, we transfected adherent GnTI$^-$ cells with 0.5 μg of plasmid DNA for each subunit and 0.2 μg of a GFP expression plasmid to identify cells for recording. For calculation of the EC_{50}, suspension GnTI$^-$ cells were virally transduced under the same conditions as were used to produce protein for crystallization. Whole-cell recordings of membrane currents were made 72 hr later at a membrane potential of −90 mV. The recordings were made with an Axopatch 200B amplifier, low-pass filtered at 5 kHz and digitized at 10 kHz using the Digidata 1440A and pClamp software (Molecular Devices). Borosilicate glass patch pipettes were pulled and polished to 2–4 MΩ resistance. The external solution contained 140 mM NaCl, 2.4 mM KCl, 4 mM $CaCl_2$, 4 mM $MgCl_2$, 10 mM HEPES (pH 7.3), and 10 mM glucose. The internal solution contained 150 mM CsF, 10 mM NaCl, 10 mM EGTA, and 20 mM HEPES (pH 7.3). The agonist ACh chloride (Sigma-Aldrich) was prepared in external solution. Solution exchange was achieved using a gravity-driven RSC-200 rapid solution changer (Bio-Logic). Dose-response relationships were fitted to normalized peak currents using the log(agonist) versus response with variable slope equation in GraphPad Prism.

Receptor Crystallization

Initial crystals were identified from protein sent to the Hauptman-Woodward Medical Research Institute high-throughput crystallization screening laboratory

(Koszelak-Rosenblum et al., 2009). Several hits were observed in their membrane protein screens that were able to be reproduced in our laboratory both in microbatch and vapor-diffusion crystallization formats. The crystals yielding diffraction shown in Figure 6C were grown at 14°C in hanging-drop format after mixing 0.5 μl of protein with 0.5 μl of reservoir solution containing 0.1 M sodium/potassium phosphate (pH 6.2), 21.5% polyethylene glycol (PEG) 1000, and 0.2 M sodium chloride. Crystals were cryoprotected by supplementing with PEG 1000 and glycerol. After a short incubation (5–30 s) in cryosolution, the crystals were flash-frozen in liquid nitrogen for X-ray diffraction analysis at the 19-ID beamline of the Advanced Photon Source.

SUPPLEMENTAL INFORMATION

Supplemental Information includes two tables and can be found with this article online at http://dx.doi.org/10.1016/j.str.2016.03.004.

AUTHOR CONTRIBUTIONS

C.L.M.P., C.M.N., and R.E.H. contributed to all aspects of the project.

ACKNOWLEDGMENTS

We thank Chris Garcia at Stanford University for providing the pVLAD6 vector, Jon Lindstrom at the University of Pennsylvania for providing nicotinic receptor subunits, Roger Tsien at UCSD for providing the mCherry gene, Henry Lester at Caltech for providing the GluCl gene, and both Alexander Sobolevsky and Peter Sims at Columbia University for helpful discussion. We thank all members of the Hibbs laboratory for feedback throughout the project and comments on the manuscript. The facility for X-ray data collection at the APS beamline 19-ID (Argonne, IL) was supported by the US Department of Energy under contract DE-AC02-06CH11357. This research project was supported by an NIH training grant (T32 NS069562) and an HHMI Gilliam Fellowship to C.L.M.P.; R.E.H. is supported by a McKnight Scholar Award, a Klingenstein-Simons Fellowship Award in the Neurosciences, The Welch Foundation (I-1812), and the NIH (R21 DA037492 and R00 NS077983).

Received: December 16, 2015
Revised: February 9, 2016
Accepted: March 4, 2016
Published: March 31, 2016

REFERENCES

Akrap, N., Seidel, T., and Barisas, B.G. (2010). Forster distances for fluorescence resonant energy transfer between mCherry and other visible fluorescent proteins. Anal. Biochem. *402*, 105–106.

Anand, R., Conroy, W.G., Schoepfer, R., Whiting, P., and Lindstrom, J. (1991). Neuronal nicotinic acetylcholine receptors expressed in Xenopus oocytes have a pentameric quaternary structure. J. Biol. Chem. *266*, 11192–11198.

Aricescu, A.R., Lu, W., and Jones, E.Y. (2006). A time- and cost-efficient system for high-level protein production in mammalian cells. Acta Crystallogr. D Biol. Crystallogr. *62*, 1243–1250.

Barrera, N.P., Herbert, P., Henderson, R.M., Martin, I.L., and Edwardson, J.M. (2005). Atomic force microscopy reveals the stoichiometry and subunit arrangement of 5-HT3 receptors. Proc. Natl. Acad. Sci. USA *102*, 12595–12600.

Bartoi, T., Augustinowski, K., Polleichtner, G., Grunder, S., and Ulbrich, M.H. (2014). Acid-sensing ion channel (ASIC) 1a/2a heteromers have a flexible 2:1/1:2 stoichiometry. Proc. Natl. Acad. Sci. USA *111*, 8281–8286.

Boyce, F.M., and Bucher, N.L. (1996). Baculovirus-mediated gene transfer into mammalian cells. Proc. Natl. Acad. Sci. USA *93*, 2348–2352.

Buisson, B., and Bertrand, D. (2001). Chronic exposure to nicotine upregulates the human (alpha)4((beta)2 nicotinic acetylcholine receptor function. J. Neurosci. *21*, 1819–1829.

Carbone, A.L., Moroni, M., Groot-Kormelink, P.J., and Bermudez, I. (2009). Pentameric concatenated (alpha4)(2)(beta2)(3) and (alpha4)(3)(beta2)(2) nicotinic acetylcholine receptors: subunit arrangement determines functional expression. Br. J. Pharmacol. *156*, 970–981.

Changeux, J.P., and Edelstein, S.J. (2005). Nicotinic Acetylcholine Receptors: From Molecular Biology to Cognition (Odile Jacob Publishing Corporation).

Chaudhary, S., Pak, J.E., Gruswitz, F., Sharma, V., and Stroud, R.M. (2012). Overexpressing human membrane proteins in stably transfected and clonal human embryonic kidney 293S cells. Nat. Protoc. *7*, 453–466.

Chun, E., Thompson, A.A., Liu, W., Roth, C.B., Griffith, M.T., Katritch, V., Kunken, J., Xu, F., Cherezov, V., Hanson, M.A., and Stevens, R.C. (2012). Fusion partner toolchest for the stabilization and crystallization of G protein-coupled receptors. Structure *20*, 967–976.

Condreay, J.P., Witherspoon, S.M., Clay, W.C., and Kost, T.A. (1999). Transient and stable gene expression in mammalian cells transduced with a recombinant baculovirus vector. Proc. Natl. Acad. Sci. USA *96*, 127–132.

Cooper, E.C., and Jan, L.Y. (2003). M-channels: neurological diseases, neuromodulation, and drug development. Arch. Neurol. *60*, 496–500.

Cooper, E., Couturier, S., and Ballivet, M. (1991). Pentameric structure and subunit stoichiometry of a neuronal nicotinic acetylcholine receptor. Nature *350*, 235–238.

Craven, K.B., and Zagotta, W.N. (2006). CNG and HCN channels: two peas, one pod. Annu. Rev. Physiol. *68*, 375–401.

Dineley, K.T., Pandya, A.A., and Yakel, J.L. (2015). Nicotinic ACh receptors as therapeutic targets in CNS disorders. Trends Pharmacol. Sci. *36*, 96–108.

Dukkipati, A., Park, H.H., Waghray, D., Fischer, S., and Garcia, K.C. (2008). BacMam system for high-level expression of recombinant soluble and membrane glycoproteins for structural studies. Protein Expr. Purif. *62*, 160–170.

Durisic, N., Godin, A.G., Wever, C.M., Heyes, C.D., Lakadamyali, M., and Dent, J.A. (2012). Stoichiometry of the human glycine receptor revealed by direct subunit counting. J. Neurosci. *32*, 12915–12920.

Engel, A.G., Shen, X.M., Selcen, D., and Sine, S.M. (2015). Congenital myasthenic syndromes: pathogenesis, diagnosis, and treatment. Lancet Neurol. *14*, 420–434.

Flint, S.J. (2009). Principles of Virology (American Society for Microbiology).

Goehring, A., Lee, C.H., Wang, K.H., Michel, J.C., Claxton, D.P., Baconguis, I., Althoff, T., Fischer, S., Garcia, K.C., and Gouaux, E. (2014). Screening and large-scale expression of membrane proteins in mammalian cells for structural studies. Nat. Protoc. *9*, 2574–2585.

Gorman, C.M., Howard, B.H., and Reeves, R. (1983). Expression of recombinant plasmids in mammalian cells is enhanced by sodium butyrate. Nucleic Acids Res. *11*, 7631–7648.

Hacker, D.L., Kiseljak, D., Rajendra, Y., Thurnheer, S., Baldi, L., and Wurm, F.M. (2013). Polyethyleneimine-based transient gene expression processes for suspension-adapted HEK-293E and CHO-DG44 cells. Protein Expr. Purif. *92*, 67–76.

Hibbs, R.E., and Gouaux, E. (2011). Principles of activation and permeation in an anion-selective Cys-loop receptor. Nature *474*, 54–60.

Hofmann, C., Sandig, V., Jennings, G., Rudolph, M., Schlag, P., and Strauss, M. (1995). Efficient gene transfer into human hepatocytes by baculovirus vectors. Proc. Natl. Acad. Sci. USA *92*, 10099–10103.

Hopkins, R., and Esposito, D. (2009). A rapid method for titrating baculovirus stocks using the Sf-9 Easy Titer cell line. Biotechniques *47*, 785–788.

Karakas, E., and Furukawa, H. (2014). Crystal structure of a heterotetrameric NMDA receptor ion channel. Science *344*, 992–997.

Kawate, T., and Gouaux, E. (2006). Fluorescence-detection size-exclusion chromatography for precrystallization screening of integral membrane proteins. Structure *14*, 673–681.

Koszelak-Rosenblum, M., Krol, A., Mozumdar, N., Wunsch, K., Ferin, A., Cook, E., Veatch, C.K., Nagel, R., Luft, J.R., Detitta, G.T., and Malkowski, M.G. (2009). Determination and application of empirically derived detergent phase boundaries to effectively crystallize membrane proteins. Protein Sci. *18*, 1828–1839.

Kuryatov, A., Luo, J., Cooper, J., and Lindstrom, J. (2005). Nicotine acts as a pharmacological chaperone to up-regulate human alpha4beta2 acetylcholine receptors. Mol. Pharmacol. *68*, 1839–1851.

Lee, C.H., Lu, W., Michel, J.C., Goehring, A., Du, J., Song, X., and Gouaux, E. (2014). NMDA receptor structures reveal subunit arrangement and pore architecture. Nature *511*, 191–197.

Lester, H.A., Xiao, C., Srinivasan, R., Son, C.D., Miwa, J., Pantoja, R., Banghart, M.R., Dougherty, D.A., Goate, A.M., and Wang, J.C. (2009). Nicotine is a selective pharmacological chaperone of acetylcholine receptor number and stoichiometry. Implications for drug discovery. AAPS J. *11*, 167–177.

Maertens, B., Spriestersbach, A., Kubicek, J., and Schafer, F. (2015). Strep-tagged protein purification. Methods Enzymol. *559*, 53–69.

Marks, M.J., Whiteaker, P., Calcaterra, J., Stitzel, J.A., Bullock, A.E., Grady, S.R., Picciotto, M.R., Changeux, J.P., and Collins, A.C. (1999). Two pharmacologically distinct components of nicotinic receptor-mediated rubidium efflux in mouse brain require the beta2 subunit. J. Pharmacol. Exp. Ther. *289*, 1090–1103.

Marks, M.J., Meinerz, N.M., Drago, J., and Collins, A.C. (2007). Gene targeting demonstrates that alpha4 nicotinic acetylcholine receptor subunits contribute to expression of diverse [^{3}H]epibatidine binding sites and components of biphasic ^{86}Rb+ efflux with high and low sensitivity to stimulation by acetylcholine. Neuropharmacology *53*, 390–405.

Marks, M.J., Meinerz, N.M., Brown, R.W., and Collins, A.C. (2010). 86Rb+ efflux mediated by alpha4beta2*-nicotinic acetylcholine receptors with high and low-sensitivity to stimulation by acetylcholine display similar agonist-induced desensitization. Biochem. Pharmacol. *80*, 1238–1251.

Meltzer, R.H., Kapoor, N., Qadri, Y.J., Anderson, S.J., Fuller, C.M., and Benos, D.J. (2007). Heteromeric assembly of acid-sensitive ion channel and epithelial sodium channel subunits. J. Biol. Chem. *282*, 25548–25559.

Miles, T.F., Dougherty, D.A., and Lester, H.A. (2013). The 5-HT3AB receptor shows an A3B2 stoichiometry at the plasma membrane. Biophys. J. *105*, 887–898.

Moroni, M., Zwart, R., Sher, E., Cassels, B.K., and Bermudez, I. (2006). alpha4beta2 nicotinic receptors with high and low acetylcholine sensitivity: pharmacology, stoichiometry, and sensitivity to long-term exposure to nicotine. Mol. Pharmacol. *70*, 755–768.

Nashmi, R., Dickinson, M.E., Mckinney, S., Jareb, M., Labarca, C., Fraser, S.E., and Lester, H.A. (2003). Assembly of alpha4beta2 nicotinic acetylcholine receptors assessed with functional fluorescently labeled subunits: effects of localization, trafficking, and nicotine-induced upregulation in clonal mammalian cells and in cultured midbrain neurons. J. Neurosci. *23*, 11554–11567.

Nelson, M.E., Kuryatov, A., Choi, C.H., Zhou, Y., and Lindstrom, J. (2003). Alternate stoichiometries of alpha4beta2 nicotinic acetylcholine receptors. Mol. Pharmacol. *63*, 332–341.

Perry, D.C., Davila-Garcia, M.I., Stockmeier, C.A., and Kellar, K.J. (1999). Increased nicotinic receptors in brains from smokers: membrane binding and autoradiography studies. J. Pharmacol. Exp. Ther. *289*, 1545–1552.

Philipps, B., Rotmann, D., Wicki, M., Mayr, L.M., and Forstner, M. (2005). Time reduction and process optimization of the baculovirus expression system for more efficient recombinant protein production in insect cells. Protein Expr. Purif. *42*, 211–218.

Qi, J., Liu, T., Pan, J., Miao, P., and Zhang, C. (2015). Rapid baculovirus titration assay based on viable cell side scatter (SSC). Anal. Chim. Acta *879*, 58–62.

Reeves, P.J., Callewaert, N., Contreras, R., and Khorana, H.G. (2002). Structure and function in rhodopsin: high-level expression of rhodopsin with restricted and homogeneous N-glycosylation by a tetracycline-inducible N-acetylglucosaminyltransferase I-negative HEK293S stable mammalian cell line. Proc. Natl. Acad. Sci. USA *99*, 13419–13424.

Robbins, J. (2001). KCNQ potassium channels: physiology, pathophysiology, and pharmacology. Pharmacol. Ther. *90*, 1–19.

Saez, J.C., Berthoud, V.M., Branes, M.C., Martinez, A.D., and Beyer, E.C. (2003). Plasma membrane channels formed by connexins: their regulation and functions. Physiol. Rev. *83*, 1359–1400.

Saul, A., Hausmann, R., Kless, A., and Nicke, A. (2013). Heteromeric assembly of P2X subunits. Front. Cell Neurosci. *7*, 250.

Seiradake, E., Zhao, Y., Lu, W., Aricescu, A.R., and Jones, E.Y. (2015). Production of cell surface and secreted glycoproteins in mammalian cells. Methods Mol. Biol. *1261*, 115–127.

Shaner, N.C., Steinbach, P.A., and Tsien, R.Y. (2005). A guide to choosing fluorescent proteins. Nat. Methods *2*, 905–909.

Shen, C.F., Meghrous, J., and Kamen, A. (2002). Quantitation of baculovirus particles by flow cytometry. J. Virol. Methods *105*, 321–330.

Sigel, E., and Steinmann, M.E. (2012). Structure, function, and modulation of GABA(A) receptors. J. Biol. Chem. *287*, 40224–40231.

Srinivasan, R., Richards, C.I., Dilworth, C., Moss, F.J., Dougherty, D.A., and Lester, H.A. (2012). Forster resonance energy transfer (FRET) correlates of altered subunit stoichiometry in cys-loop receptors, exemplified by nicotinic alpha4beta2. Int. J. Mol. Sci. *13*, 10022–10040.

Traynelis, S.F., Wollmuth, L.P., Mcbain, C.J., Menniti, F.S., Vance, K.M., Ogden, K.K., Hansen, K.B., Yuan, H., Myers, S.J., and Dingledine, R. (2010). Glutamate receptor ion channels: structure, regulation, and function. Pharmacol. Rev. *62*, 405–496.

Wang, W., Cheng, T., Ma, K., Xia, D., Wang, Y., Liu, J., Du, H., Shih, J.W., Zhang, J., Zhao, Q., and Xia, N. (2013). Development of a novel baculovirus titration method using the enzyme-linked immunosorbent spot (ELISPOT) assay. J. Virol. Methods *188*, 114–120.

Yang, Z., Taran, E., Webb, T.I., and Lynch, J.W. (2012). Stoichiometry and subunit arrangement of alpha1beta glycine receptors as determined by atomic force microscopy. Biochemistry *51*, 5229–5231.

Zhou, Y., Nelson, M.E., Kuryatov, A., Choi, C., Cooper, J., and Lindstrom, J. (2003). Human alpha4beta2 acetylcholine receptors formed from linked subunits. J. Neurosci. *23*, 9004–9015.

Zwart, R., and Vijverberg, H.P. (1998). Four pharmacologically distinct subtypes of alpha4beta2 nicotinic acetylcholine receptor expressed in *Xenopus laevis* oocytes. Mol. Pharmacol. *54*, 1124–1131.